International Journal of Applied Earth Observation and Geoinformation 122 (2023) 103412

Contents lists available at ScienceDirect

International Journal of Applied Earth Observation and Geoinformation

journal homepage: www.elsevier.com/locate/jag

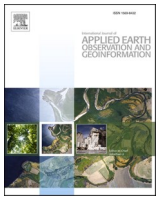

# A Bi-LSTM approach for modelling movement uncertainty of crowdsourced human trajectories under complex urban environments

Yue Yu [a,e,1], Yepeng Yao [b,1], Zhewei Liu [c,e,*], Zhenlin An [d], Biyu Chen [e], Liang Chen [e], Ruizhi Chen [e]

[a] Department of Land Surveying and Geo-Informatics, The Hong Kong Polytechnic University, 999077, Hong Kong, China
[b] The Planning Department, The Government of the Hong Kong SAR, 999077, Hong Kong, China
[c] UrbanResilience.AI Lab, Zachry Department of Civil and Environmental Engineering, Texas A&M University, College Station, TX, 77843, United States
[d] Department of Computing, The Hong Kong Polytechnic University, 999077, Hong Kong, China
[e] State Key Laboratory of Information Engineering in Surveying, Mapping and Remote Sensing (LIESMARS), Wuhan University, Wuhan 430000, China

ARTICLE INFO

*Keywords:*
Movement uncertainty
Crowdsourced human trajectories
Pedestrian motion detection
GNSS

ABSTRACT

Modelling the movement uncertainty of crowdsourced human trajectories in complex urban areas is useful for various human mobility analytics and applications. However, the existing human movement uncertainty modelling approaches only consider the largest movement distance or speed, and fixed sampling and measurement errors, resulting in limited accuracy in uncertainty prediction. To fill this gap, this paper presents a Bi-directional Long Short-Term Memory (Bi-LSTM) assisted framework for modelling the uncertainty of crowdsourced human trajectories under complex urban environments. The proposed movement uncertainty modelling framework adaptively integrates the pedestrian motion detection characteristics, including the real-time gait-length and heading deviation features under detected step period. The characteristics are further combined with the Global Navigation Satellite System (GNSS) originated location, speed and virtual heading information and constructed as the input features for the uncertainty prediction model. Comparison with the existing uncertainty modelling methods is conducted using the real-world datasets, and the results demonstrate the presented Bi-LSTM assisted framework's robust outperformance in achieving more adaptive and accurate movement uncertainty prediction, as measured by multiple metrics. This study provides an accurate and practical solution for modelling the movement uncertainty of human trajectories under complex urban areas, and can support reliable analytics for crowdsourced urban big data.

## 1. Introduction

The crowdsourced human trajectory data is an essential part for urban big data analytics, which can effectively represent the spatial-temporal mobility and activity of the population. With the support of mobility tracking sensors, various terminal devices are capable of acquiring rich crowdsourced motion information from users, which can be further applied for various developments of location-based services (LBSs), such as a network planning system (Tu et al., 2020), user behavior analytics (Liu et al., 2022; Liu et al., 2022), urban risk forecast (Huang et al., 2022), and intelligent logistics (Liu et al., 2020; Shi et al., 2021). In practice, the pedestrian trajectories collected with terminal devices often deviate from the pedestrians' ground-truth trajectories, and the deviations (termed as movement uncertainty in this study) vary from place to place due to the complex urban environments. Such movement uncertainty poses great threats on the accuracy of mobility analytics and seriously undermines the effectiveness of trajectory-associated feature extraction and related real-world applications (Rossi et al., 2021; Liu et al., 2022). A growing number of researches have been conducted on how to represent and handle trajectory uncertainty from huge amounts of mobile sensing data in changeable and disturbed scenarios, which are especially common among work on trajectory mining, prediction, and spatial query (Liu et al., 2021; Liu et al., 2021; Yu et al., 2021; Liu et al., 2018).

Typically, the gathered two-dimensional (2D) trajectory can be modelled as a finite vector of time-related position coordinates $< \mathbf{rt}_1$,

* Corresponding author.
*E-mail address:* zheweiliu@tamu.edu (Z. Liu).
[1] Yue Yu and Yepeng Yao contribute equally to this paper.

https://doi.org/10.1016/j.jag.2023.103412
Received 5 April 2023; Received in revised form 27 June 2023; Accepted 1 July 2023
Available online 6 July 2023

$\mathbf{rt}_2$,…, $\mathbf{rt}_n$>, provided by different types of measurement devices where $\mathbf{rt} = (x, y, t)$ denotes the specific 2D position and matching timestamp $t$ (Shi et al., 2022). In real-world situations, sampling and measurement errors are two main sources that contribute to the uncertainty of the human movement trajectory. The discontinuous location data points normally have varying sampling rates, and the corresponding sampling error is caused by the missed motion information among the collected adjacent GNSS locations (Zheng, 2012). The measurement error occurs during the data-gathering process and is related to the used localization strategy, the flexible application contexts, and the variance in hardware precision and signal processing algorithms (Zheng et al., 2014; Zheng, 2015).

The potential path area (PPA) and the concept of space–time prism (STP) are traditionally used for delineating the trajectories' movement uncertainty (Miller, 1991; Kwan, 1998). Previous researchers utilized either the walking velocity or the movement length of the vehicle/ pedestrian to evaluate the PPA in most situations. However, the premise of such uncertainty estimates was based on the objects' constant velocity, which would cause the overestimated PPA in real-world practices (Xia et al., 2018; Downs and Horner, 2014). The researchers established adaptive velocity control criteria to achieve a more effective PPA modelling result by reducing the impact of velocity calculation deviation in the PPA prediction (Zhou et al., 2018). In addition to the movement speed, the moving distance, also demonstrates important in PPA prediction. In the enhanced approximate upper bound (AUB) model presented by Furtado et al. (Furtado, 2018), the maximum moving distance is used to estimate the uncertainty area, and the Manhattan distance is used to present the maximum movement length for extensive comparison with the approaches based on Euclidean distance. The randomness and complexity of human trajectory features and movement paths hindered the effectiveness of Manhattan distance for capturing the relationship among sample points. The varying sampling rate and the constant measure inaccuracy are usually taken into consideration to model the uncertainty of the predicted potential PPA area.

Previous studies have revealed that the existing uncertainty modeling techniques primarily focus on fixed sampling rates and constant measurement errors. Aiming at the pedestrian mobility analytics under complex urban areas, various factors usually affect the accuracy of collected pedestrian trajectories such as the occlusion/ reflection of acquired GNSS signals, and pedestrian movement patterns, which highlight the following challenges remaining to be solved: 1) Complex relationships between human motion, GNSS information, and ground-truth trajectory: In urban areas, the GNSS reported location usually deviates from the ground-truth trajectory due to the signal occlusion and reflection. Therefore, how to comprehensively consider the relationship between human motion data and GNSS data for uncertainty prediction is an essential task (Yu et al., 2022); 2) Changeable sampling rates among different locations: Due to the complex urban environments, the real-time collected location-related data is not consistent in terms of the set sampling rate, and the discontinuous movement sampling leads to the larger uncertainty error (Ruizhi and Liang, 2017); 3) Varied measurement errors at reported GNSS locations: Due to the signal occlusion and reflection in the complex urban contexts, the GNSS reported locations usually suffer from harsh and location-dependent measurement errors (Wen and Hsu, 2022); 4) Disordered crowdsourced human trajectories: Because of the randomness of pedestrian movement, pedestrian trajectories are typically disordered as opposed to those of vehicles or robots, makes modeling the uncertainty of real-world human trajectories more challenging (Li et al., 2021).

Consequently, to address the above challenges, this study presents a novel framework to accurately capture the movement uncertainty of crowdsourced human trajectories in complex urban environments, through a cutting-edge deep-learning approach. This paper uses the previous locations updated by pedestrians, and includes the relationship between motion information and GNSS-originated speed and distance change information, to construct a sequence of context, which is then adopted as the input vector of the Bi-directional Long Short-Term Memory (Bi-LSTM) assisted uncertainty prediction model to obtain the final uncertainty error and uncertainty region. Additionally, the Euclidean distance between ground-truth trajectory and GNSS-based trajectory is chosen as the training model's output value, and the Euclidean distance coefficient is adaptively chosen based on the expected outcomes during the training phase. This work extracts several elements from the human trajectory data to represent the variable measurement and sampling errors. The anticipated Euclidean distance is then used to generate the uncertainty area in accordance with the results of the movement uncertainty prediction. A thorough evaluation of the proposed Bi-LSTM-based uncertainty prediction framework using our generated real-world trajectory datasets demonstrate the model's effectiveness, and the comparison results with state-of-the-art algorithms further highlight its precision and robustness in the area of human trajectory's movement uncertainty modeling for real-world application under different scenes.

The innovations of this work are described as follows:

(1) Instead of merely considering collected GNSS points and extracted features for analyzing uncertainty, this paper also combines complex human motion information within a time period of adjacent GNSS points. The corresponding relationship between human motion and GNSS updates is also modeled in the feature vector, which can provide richer and more continuous pedestrian motion information under weak GNSS or GNSS-denied urban scenes.
(2) This work presents a novel Bi-directional Long Short-Term Memory (Bi-LSTM) framework for uncertainty prediction by considering all potential influence factors of collected human trajectory. In contrast to the conventional approaches, a succession of human motions and GNSS-reported location points over a brief period of time are regarded as the determining factors to accurately present the time–space relevance of the uncertainty of human movement trajectory.
(3) This paper generates the real-world training and test datasets with the baseline reference provided by simultaneous localization and mapping (SLAM) technology. The generated training dataset contains both time-varying measurement error and time-varying sampling error, and complex pedestrian motion information is also collected and modeled to enhance the precision of the uncertainty error modelling.
(4) The uncertainty error of collected trajectory point provided by the reported GNSS in this work is presented as adaptive Euclidean distance, and the Euclidean distance coefficient is adaptively chosen in accordance with the training output. Under various pedestrian motion modes, the uncertainty area is finally determined by accounting for both sampling error and measurement errors.

The structure of this paper is described as follows: Our problem statement, dataset generation, and suggested methodology are all covered in Section 2. The findings of our experiment are presented in Section 3 to demonstrate the efficacy and reliability of our method. The novelty and limitations of our work are presented in Section 4. The entire research is concluded in Section 5, which also outlines some possible real-world applications for our approach.

## 2. Problem statement, dataset and methodology

The fundamental obstacles for movement uncertainty prediction of pedestrian trajectories under large-scale urban areas are covered in this part, along with the preparation and description of a real-world dataset for training purposes. Eventually, a comprehensive and successful methodology based on deep learning is provided to address the identified issues.

### 2.1. Problem statement

Our effort aims to provide a thorough and reliable model for pedestrian movement uncertainty in intricate urban context. The model considers the changing human motion, sampling and measurement errors at the same time, and provides an adaptive uncertainty error prediction scheme in order to comprehensively present these changing errors caused by different location sources and their time-related influence factors. The important terms linked to this issue are provided as follow:

**Definition 1**. *Space-time location point. One location in time and space STP is a 2D geo-spatial point under specific time period that is provided by various positioning techniques, described as* $STP_i = (x, y, t)$, *in which* $(x,y)$ *and* $t$ *denote the geo-spatial location point and corresponding timestamp.*

**Definition 2**. *Ground-truth trajectory GT provided by SLAM techniques. The ground-truth trajectory* $GT = \{GT.STP_1, GT.STP_2, ..., GT.STP_n\}$ *indicates a modeled STP set that contains the pedestrian's reference locations. The ground-truth trajectory in this work is acquired using the combination of SLAM system and the open street map, and the centi-meter level reference trajectory can be acquired for error comparison purposes.*

**Definition 3**. *GNSS-based trajectory HT provided by hybrid location sources: In this work, human motion detection is applied in GNSS signal-denied areas to enhance the trajectory continuity. A human motion assisted GNSS trajectory HT is a collection of indexed STPs that approximates an individual's trajectory* $HT = \{HT.STP_1, HT.STP_2, ..., HT.STP_n\}$ *by using human motion detection techniques in a temporary time period when the GNSS signal is missing, where* $HT.STP_n$ *is the continuous reconstructed trajectory point corresponds to* $GT.STP_n$.

The following part is how we present our study of modeling the movement uncertainty of pedestrian trajectories under complex urban environments:

Problems of crowdsourced pedestrian movement uncertainty under complex urban environments:

(1) Different from the outdoor trajectories under open area with continuous GNSS-reported position points with fixed sampling rate and nearly constant measurement error, the first challenge towards the trajectory acquisition under complex urban areas is that limited GNSS locations are included, and the measurement error of GNSS signals are changing over time, therefore the human motion detection algorithm is required to compensate the performance of limited GNSS points.
(2) Besides, aiming at connecting the ground-truth trajectory *GT* and human motion assisted GNSS trajectory *HT* for further uncertainty model training, we need to discover the time and spatial relationship *M* between *GT*, *HT,* and Dis($GT.STP_i$, $HT.STP_i$), in which $M : HT \rightarrow Dis(GT.STP_i, HT.STP_i)$, and Dis($GT.STP_i$, $GT.STP_i$) represents the calculated Euclidean distance among each pair of $GT.STP_i$ and $HT.STP_i$.
(3) Our human motion assisted GNSS trajectory *HT*, in contrast to conventional acquired GNSS trajectories that lack timestamp information, is able to acquire comprehensive location points in which each point has corresponding ground-truth location reference (e.g., $HT.STP_i.t = GT.STP_i.t$), allowing calculation of the difference among $HT.STP_i$ and $GT.STP_i$ under the case of time-varying sampling and measurement errors.

### 2.2. Dataset collection for ground-truth and GNSS-based trajectories

The crowdsourced human trajectories in this study are respectively collected from two approaches: (1) the GNSS-based trajectory HT is collected using hybrid location sources including single GNSS and motion tracking sensors (2) the ground-truth trajectory GT is collected based on the assistance of SLAM system, which can acquire centimeter level moving trajectory. Details are given below.

#### 2.2.1. Collection of GNSS-based trajectory HT

In order to generate a more comprehensive and continuous GNSS-based trajectory HT, in this case, the pedestrian's movement trajectory is modeled as a graph by considering both GNSS reported locations and corresponding human motion data extracted between adjacent GNSS location periods, which is described in Fig. 1:

Fig. 1 shows how to rebuild the GNSS-based trajectory HT, and the recorded gait-length and direction vector $\{\{\theta_1^{i-1|i}, L_1^{i-1|i}\}, \cdots, \{\theta_m^{i-1|i}, L_m^{i-1|i}\}\}$ among each two separate spatiotemporal locations are included in the pedestrian motion information. The GNSS reported positions are served as the node points of the graph, and the recorded gait-length and direction information between two adjacent spatiotemporal locations are provided by extracted human motion features.

To provide reliable human motion features for the whole trajectory graph, the effects of handheld modes of the mobile terminals need to be detected and compensated. In this work, the typical handheld modes are divided into four kinds: reading, calling, swaying, and pocket. The various handheld modes are initially identified and categorized using sensors-based features via machine learning techniques, and sensors data acquired from all the detected handheld modes are converted into basic reading mode for further trajectory recreation (Yu et al., 2022). Fig. 2 illustrates the four distinct smartphone handheld modes:

After the handheld mode detection and conversion, the entire trajectory can be recreated as follows utilizing the motion data gathered throughout the trajectory period:

$$STP_i(L_i, \theta_i) = R_{01} + \sum_{i=1}^{n} \begin{bmatrix} L_i cos(\theta_i) \\ L_i sin(\theta_i) \end{bmatrix} \quad (1)$$

where $R_{01}$ denotes the chosen trajectory's first point. The acquired step-length and direction data among two nearby spatiotemporal sites, represented by $L_i$ and $\theta_i$, can be calculated by (Yu et al., 2022).

#### 2.2.2. Collection of ground-truth trajectory GT

In addition, to provide the ground-truth trajectory reference, simultaneous localization and mapping (SLAM) system is applied to provide centi-meter level reference trajectory using the intelligent fusion structure of high-precision light detection and ranging (Lidar), inertial sensors, and visual based location sources. Such system has been verified to be capable of capturing human trajectories at centimeter-level accuracy (Bao et al., 2022). Besides, the smartphone is held under different handheld modes in the procedure of dataset collection, which is described in Fig. 3:

Overall, the final created dataset includes the following information:

$$Vector_{train} = \left\{x_{G/O}, y_{G/O}, L, \theta, x_r, y_r\right\} \quad (2)$$

Where $Vector_{train}$ indicates each basic unit in the generated training dataset, $x_{G/O}$ and $y_{G/O}$ indicate the ground-truth location reference, $L$ and $\theta$ represent the gait-length and heading information, $x_r$ and $y_r$ are $x$ and $y$ coordinates of GNSS-based trajectory.

### 2.3. Features construction for movement uncertainty prediction

To predict the movement uncertainty, this work constructs multi-dimensional features based on detected human motion modes and GNSS signals. The details of the constructed features are described as below:

(1) Actual sampling interval of adjacent GNSS location $T_i$ and GNSS reported location $\{x_G(k), y_G(k)\}$ at current timestamp.
(2) Acquired gait-length and heading vector among two adjacent GNSS calculated locations, in which the gait and heading information is provided by (Yu et al., 2022):

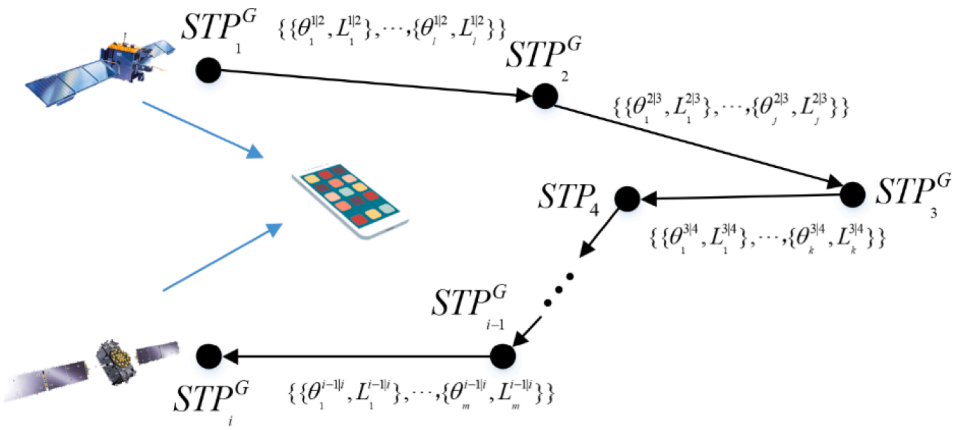


**Fig. 1.** Description of graph-based GNSS-based trajectory HT.

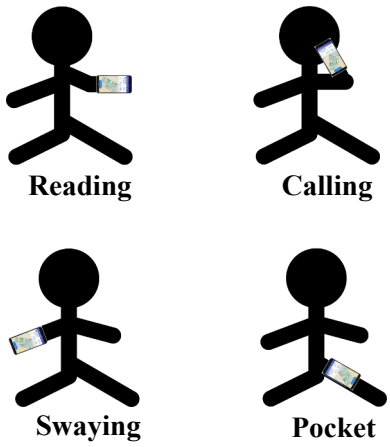


**Fig. 2.** Different handheld modes.

**Fig. 3.** The SLAM system in this study for dataset generation.

$$R_{k|k-1} = \begin{pmatrix} \varsigma_1^{W/G} & \vartheta_1^{W/G} \\ \varsigma_2^{W/G} & \vartheta_2^{W/G} \\ \cdots & \cdots \\ \varsigma_N^{W/G} & \vartheta_N^{W/G} \end{pmatrix} \tag{3}$$

where $N$ indicates the amounts of steps detected among adjacent GNSS locations,$\varsigma_N^{W/G}$ and $\vartheta_N^{W/G}$ indicate the corresponding step-length and heading vector.

(3) Coordinate differences provided by human motion detection, GNSS, and hybrid value under x-axis and y-axis:

$$\begin{cases} \Delta X_k^M = \sum_{i=1}^{N} \varsigma_i \cdot \cos(\vartheta_i) \\ \Delta Y_k^M = \sum_{i=1}^{N} \varsigma_i \cdot sin(\vartheta_i) \\ \Delta X_k^G = x_G(k) - x_G(k-1) \\ \Delta Y_k^G = y_G(k) - y_G(k-1) \\ \Delta X_k^{G-M} = x_G(k) - \sum_{i=1}^{N} \varsigma_i \cdot \cos(\vartheta_i) \\ \Delta Y_k^{G-M} = y_G(k) - \sum_{i=1}^{N} \varsigma_i \cdot sin(\vartheta_i) \end{cases} \tag{4}$$

(4) Euclidean distance of adjacent GNSS based location source and gait and heading originated based location source:

$$\begin{cases} D_k^M = \sqrt{\left(\sum_{i=1}^{N} \varsigma_i \cdot \cos(\vartheta_i)\right)^2 + \left(\sum_{i=1}^{N} \varsigma_i \cdot sin(\vartheta_i)\right)^2} \\ D_k^{GNSS} = \sqrt{\left(x_G(k) - x_G(k-1)\right)^2 + \left(y_G(k) - y_G(k-1)\right)^2} \end{cases} \tag{5}$$

Where $\{x_G(k), y_G(k)\}$ represents the GNSS-originated locations.

(5) Estimated GNSS-originated speed and location observations and gait and heading originated observations:

$$\begin{cases} v_k^M = D_k^M / \varepsilon_k^{GNSS} \\ v_k^{GNSS} = D_k^{GNSS} / \varepsilon_k^{GNSS} \end{cases} \tag{6}$$

where $v_k^M$ and $v_k^{GNSS}$ represent the MEMS sensors and GNSS originated walking speeds. $\varepsilon_k^{GNSS}$ indicates the sampling intervals of GNSS based location source.

(6) Virtual heading observations calculated by gait and heading information and GNSS locations:

$$\begin{cases} \xi^{M}_{virtual}(k) = \arccos\left(\dfrac{\sum_{i=1}^{M}\varsigma_i \cdot sin(\vartheta_i)}{\sum_{i=1}^{M}\varsigma_i \cdot \cos(\vartheta_i)}\right) \\ \xi^{GNSS}_{virtual}(k) = \arctan\left(\dfrac{x_G(k) - x_G(k-1)}{y_G(k) - y_G(k-1)}\right) \end{cases} \tag{7}$$

where $\xi^{M}_{virtual}(k)$ and $\xi^{GNSS}_{virtual}(k)$ represent the GNSS-originated virtual heading among adjacent step periods as well as the gait and heading originated virtual heading.

(7) Average signal-to-noise ratio (SNR) of GNSS signals: For urban navigation, the SNR characteristic is able to efficiently describe the degree of GNSS signal influence. The mean SNR value is used as the input feature in this work (Yu et al., 2022):

$$SNR_{mean}(k) = \frac{\sum_{\eta=1}^{\alpha} SNR_{\eta}(k)}{\alpha} \tag{8}$$

where $\alpha$ indicates the amounts of observed satellites,$SNR_{\eta}(k)$ represents the acquired SNR of corresponding satellite.

### 2.4. Proposed Bi-LSTM based model for movement uncertainty prediction

This work applied a hybrid Bi-LSTM and multilayer perceptron (MLP) network for autonomous uncertainty error prediction using the constructed trajectory features in Section 2.3. Since the LSTM-based deep learning network can effectively predict the data of the next moment based on the data of the previous period, it is very suitable for continuous pedestrian trajectory. The LSTM unit has limitations, despite its ability to process past information, it cannot use future data for prediction. To overcome the limitations of LSTM units, the researchers proposed Bi-LSTM, which consists of two different LSTM hidden layers with opposite output directions. Under this structure, both previous and future information can be leveraged at the output layer. Bi-LSTM has the advantage that LSTM does not have, so the experiments described in this paper also include the model performance comparison of Bi-LSTM and LSTM networks. The extracted trajectory features described in Section 2.3 are modeled as the input vector of the proposed Bi-LSTM network, which is described in Fig. 4:

In the proposed Bi-LSTM model, the parameters of single LSTM unit are presented as follows (Liu et al., 2022):

$$\begin{cases} f_t = \sigma\cdot(W_f\cdot h_{t-1} + U_f\cdot X_t + b_f) \\ i_t = \sigma\cdot(W_i\cdot h_{t-1} + U_i\cdot X_t + b_i) \\ a_t = tanh(W_a\cdot h_{t-1} + U_a\cdot X_t + b_a) \\ \widetilde{C}_t = \widetilde{C}_{t-1} \bullet f_t + i_t \bullet a_t \\ o_t = \sigma\cdot(W_o\cdot h_{t-1} + U_o\cdot X_t + b_o) \\ h_t = o_t\cdot tanh(C_t) \\ \widehat{y}_t = \sigma(Vh_t + c) \end{cases} \tag{9}$$

where $i_t$, $f_t$, $o_t$ indicate the input, forget and output units,$X_t$ is the modeled input vector of network in each input phase $t$ according to the constructed trajectory features in Section 2.3, and the $h_t$ represents the hidden state vector, which is modeled as the output of overall network. $\sigma$ indicates the sigmoid function, and $C_t$ is the memorized state at the moment $t$, candidate vector is mixed with output vector.

The output layer of the proposed Bi-LSTM units is simulated as the input vector of the MLP network:

$$\widehat{E}_i = MLP(y_i) \tag{10}$$

Finally, as the output vector of developed uncertainty evaluation algorithm, the movement uncertainty error $\widehat{E}_i$ is presented as the deviation between the acquired GNSS location and ground-truth reference location $Dis(GT.\ STP_i, HT.\ STP_i)$.

## 3. Experimental results

In this section, the comprehensive experiments and accuracy measurements are presented to evaluate the performance of proposed Bi-LSTM-based movement uncertainty modelling framework. In addition, the uncertainty region for the selected trajectory is generated based on the predicted uncertainty error, and the developed framework is also compared with state-of-the-art uncertainty prediction models under different accuracy measurements using the real-world dataset.

### 3.1. Dataset collection and model settings

Our dataset is collected in the open campus of The Hong Kong Polytechnic University, in which the received GNSS signal is seriously influenced by the reflection, occlusion and causes the time-varying sampling errors and large measurement errors, as shown in Fig. 5. The ground-truth trajectories of individuals are obtained by using SLAM system described in Fig. 3, which can survey location with centimeter-level accuracy. The GNSS-based trajectory HT contains human motions and locations are recorded with various kinds of smartphones including Google Pixel 3,4, Huawei P30, Samsung A7, and Xiaomi Mi 10. In this study, there are 15 trajectories (7,954 points) in totally collected, and some typical test routes in the constructed dataset are described in Fig. 6:

Fig. 6 indicates that the raw collected GNSS-based trajectories prove large measurement error compared with ground-truth trajectories. To

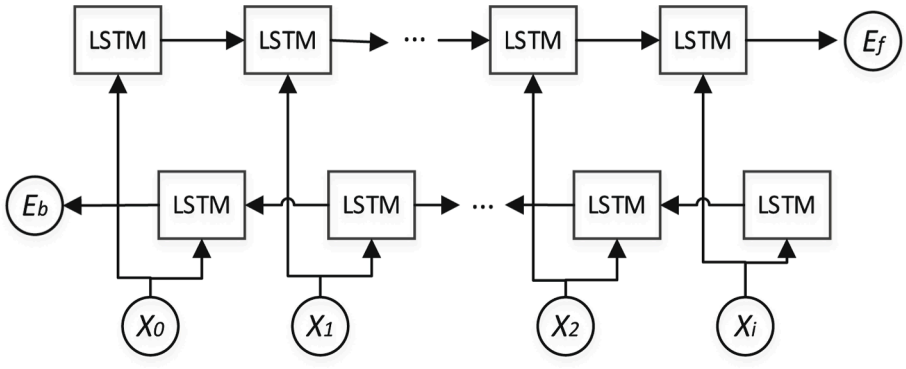


**Fig. 4.** Structure of Proposed Bi-LSTM Network.

**Fig. 5.** Experimental environments for data collection.

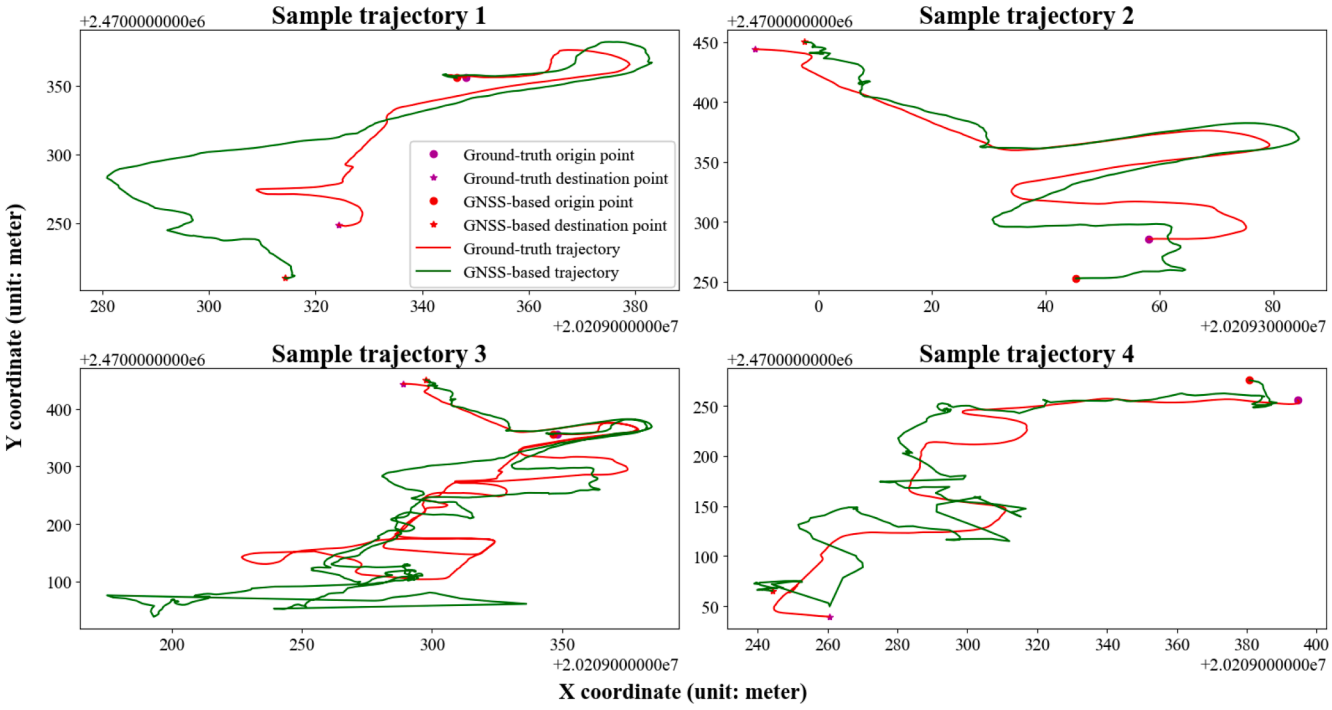


**Fig. 6.** Several sample trajectories out of the 15 experiment trajectories.

**Table 1**
Statistics of the Experiment Dataset.

| Number of trajectories | Total number of recorded points | Averagetrajectorylength (meter) | Maximum speed (m/s) | Average speed (m/s) | Average sampling interval (second) |
|---|---|---|---|---|---|
| 15 | 7,954 | 981.7 | 55.6 | 1.7 | 1.1 |

evaluate the performance of our final trained model, in our experiments 70 % of the 7,954 GNSS points are applied for model training and the other 30 % are applied as the test dataset. The statistics of the generated dataset are displayed in Table 1.

The resulting dataset created in our paper encompasses over 15 trajectories and 7,954 spatiotemporal points, as shown in Table 1. The obtained trajectories also feature a variety of real-time sampling intervals due to the effects of complex environments, and the average sampling rate reaches 1.1 Hz using smartphones.

In the proposed Bi-LSTM framework, the model setting uses the Adam as the optimizer due to its effectiveness with regards to a sizable training dataset. The dimension of the input vector in the deep learning structure is set to 14, while the final unit's hidden state's dimension is set to 80. In each training phase, a length of 20 continuous vector is applied as input vector. According to sensitivity analysis, the aforementioned parameters can, generally speaking, accurately present the model's average performance when utilizing various values.

To evaluate the effectiveness of the selected Bi-LSTM model for movement uncertainty prediction, three classical models including Long Short-Term Memory (LSTM) (Liu et al., 2022), 1D Convolutional Neural Network (1D-CNN) (Shi et al., 2022), Multilayer perceptron (MLP) (Yu et al., 2021), are applied for comparison purposes under the same settings such as the optimizer, training number, training dataset, length of input features. The evaluated average prediction error using the same test dataset is described in Fig. 7:

Fig. 7 represents that the developed Bi-LSTM model realizes higher uncertainty prediction precision compared with three different types of networks, and the Cumulative Distribution Function (CDF) of prediction error is lower than 2.04 m in more than 75 % values, compared with LSTM, MLP, and 1D-CNN with 2.46 m, 3.12 m, 4.48 m in more than 75 % values, respectively.

### 3.2. Baseline models and evaluations

This study selects three baseline models for performance comparison: (1) UB, which is a classic model for creating elliptic uncertainty regions by considering trajectories' starting/ending points, moving time and maximum moving speed (Li et al., 2018; Lu et al., 2016); (2) AUB proposed by (Furtado, 2018), which introduced the concept "Approximate Upper Bound Distance" to limit the size of elliptic region; (3) BAEE produced by (Shi et al., 2021), which extends AUB by including Minkowski distance metric. The maximum speed of UB is set as 55.6 m/s with reference to Table 1, and p value for BAEE is set as 1.5.

To perform a quantitative comparison the performance of existing models and our proposed Bi-LSTM approach, the following metrics are

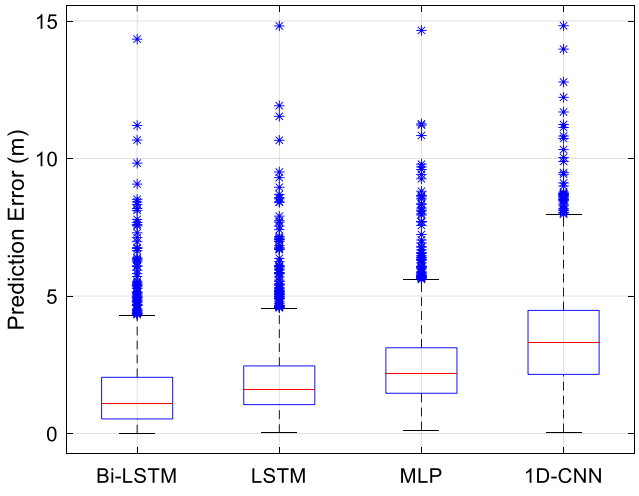


**Fig. 7.** Prediction errors comparison of different models.

adopted: (1) the coverage ratio, which represents the proportion of the ground-truth trajectories covered by the uncertain regions, to evaluate the completeness of the uncertain regions. (2) the mean absolute error (MAE) between the predicted trajectory uncertainty error and the actual trajectory uncertainty error between the ground-truth trajectory point and the corresponding GNSS-based trajectory point, for evaluating the preciseness of the methods. The uncertainty errors of the models should be able to reflect the distance between the ground-truth trajectory points and the GNSS trajectory points. For the comparison methods (i.e., UB, AUB and BAEE), the locations of ground-truth trajectory points are delimited within the elliptic uncertainty regions. Consequently, the predicted uncertainty errors are defined as the average Euclidean distance from all the points on the boundary of elliptic uncertainty regions to the corresponding GNSS trajectory point (i.e., the focus of the ellipse), which corresponds to the length of the ellipse's semi-major axis (https://studylib.net/doc/5866728/the-average-distance-in-an-ellipse).

### 3.3. Performance evaluation

The uncertain regions of our method and the baseline models are generated on the 15 experimental trajectories. For our model, the uncertain regions are built by creating a set of circles, with each point at the GNSS-based trajectory as center and the predicted uncertainty error, as radius. Fig. 8 shows our method's uncertain regions on several sample trajectories.

We further evaluate the performance of our method against the baseline models for each trajectory. A snapshot of the uncertain regions by respective methods is shown in Fig. 9. The shapes and covered areas by the uncertain regions vary among the models.

The uncertain region aims to specify a spatial range where the ground-truth trajectories fall in. Consequently, it's desirable that the uncertain regions can have complete coverage of the ground-truth trajectories. To measure the regions' completeness, the coverage ratios (see Section 3.2) of respective method on each trajectory are shown in Table 2. The results show that compared with baseline models like BAEE and AUB, our method can achieve significantly more thorough coverage ratio. For most of the experimental trajectories, coverage ratio by our method is achieved at more than 95 %. The average coverage ratio of our method over all the trajectories is 98.1 %, which is considerably better than those of BAEE and AUB (i.e., 68.2 % and 38.2 %). In contrast, UB can also yield very high coverage ratio, which is 97.9 %, slightly lower than our method. These results demonstrate that our method provides more comprehensive coverage of the ground-truth trajectories in the uncertain regions, surpassing the baseline methods in terms of completeness.

Notably, the coverage ratios of the methods are generally directly affected by the areas of the generated uncertain regions, meaning that the larger the uncertain region's area is, the more ground-truth trajectory points can be covered (better completeness). However, as the uncertain region's area keeps increasing, it provides less information about the actual deviations between the GNSS-based and ground-truth trajectories, and becomes less precise in indicating the actual locations of ground-truth trajectories. Consequently, an ideal uncertain region should have a balanced trade-off between completeness and precision. Table 3 shows the MAE achieved by respective methods on each trajectory. With reference to Fig. 9 and Table 3, it can be seen that although the high coverage ratio by UB is mainly due to the large area of the generated uncertain regions, which in turn leads to UB's being less informative in indicating the actual locations of the ground-truth trajectory and undermined precision (high MAE). The results show that the MAE by our method is substantially less than those by the baseline methods. The average MAE values by baseline methods are 16.30, 17.23 and 40.00 (for BAEE, AUB and UB respectively), significantly larger than that of our method 1.82, demonstrating our method's remarkable outperformance in accurately predicting the uncertainty error between the GNSS-based trajectories and ground-truth trajectories (better precision),

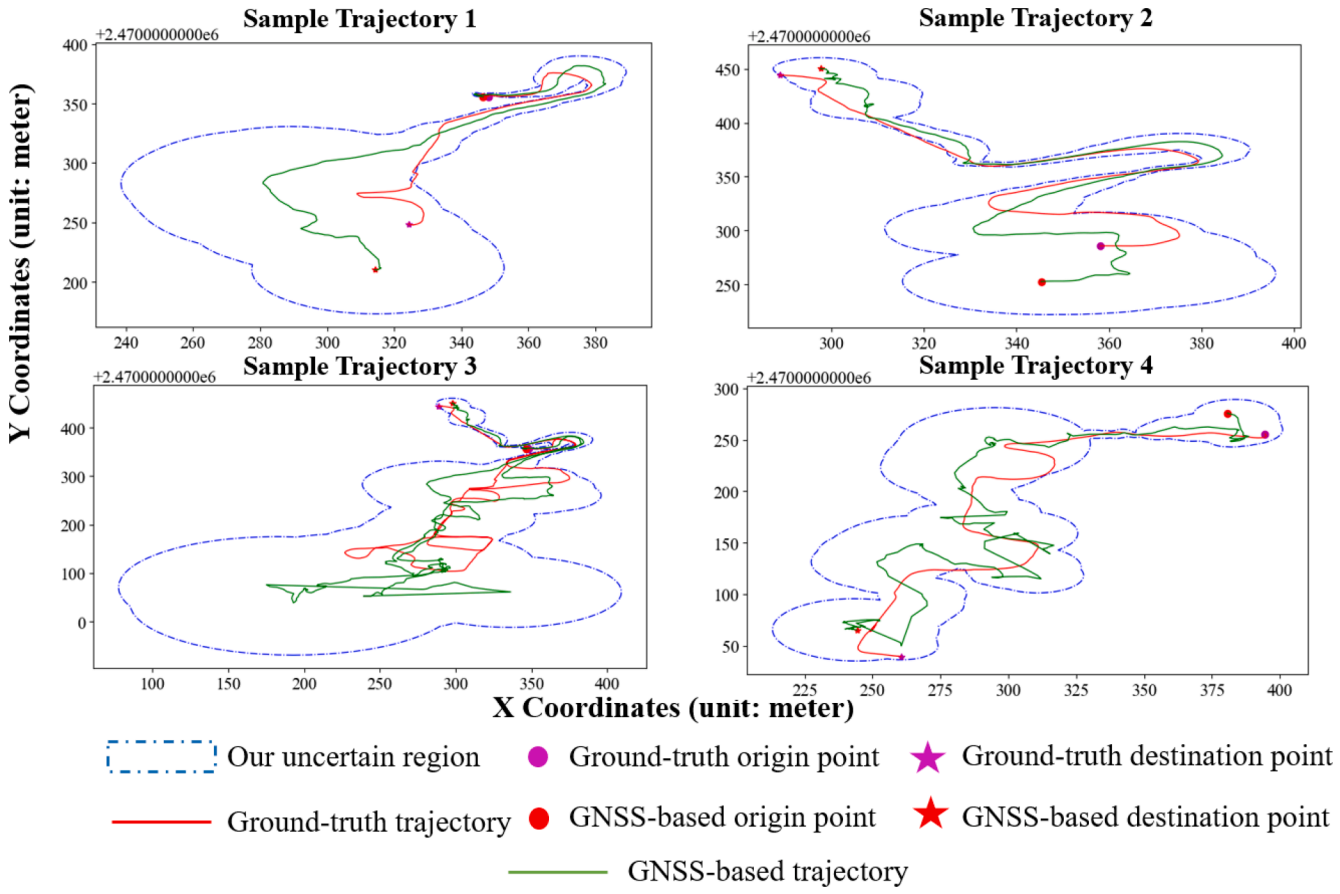


**Fig. 8.** The uncertain regions generated by our methods on several sample trajectories.

over baseline methods.

### 3.4. Hyperparameter sensitivity analysis

To assess the robustness of our model, we also investigate the influence of two important hyperparameter selections, namely (1) the features of how many previous locations should be included to predict the deviation at the current location, (2) the output dimension of the final Bi-LSTM unit, which are termed as *k_steps* and *output_dimen* respectively here. The hyperparameter combinations were searched in the space (k_steps $\in$ (Liu et al., 2018; https://studylib.net/doc/5866728/the-average-distance-in-an-ellipse) $\times$ output_dimen $\in$ [60,100]) and the MAE (see Section 3.2) is used as the measurement for model performance. As displayed in Fig. 10, the results show that, with different hyperparameter selections, the MAE by our model ranges from [0.66, 2.35] and the mean is 1.12. Especially, the yielded MAE of our model decreases as the k_steps increase, which marks the model performance improvement and may be possibly due to the more comprehensive information included in the model. Such results demonstrate that our model can yield robust as well as better performance, compared with comparison methods' MAE as in Table 3.

## 4. Discussion

In this section, a comprehensive discussion is conducted, focusing on the advantages and disadvantages of our proposed Bi-LSTM based movement uncertainty modelling approach.

### 4.1. Adaptive prediction of GNSS positional errors

Predicting the GNSS positional errors in urban context has been a longstanding and complex problem. Urban structures, such as tall buildings, can obstruct the direct line-of-sight between GNSS satellites and receivers, which can cause a weaker or distorted signal and GNSS errors. Besides, when GNSS signals are reflected off nearby surfaces, such as buildings or large vehicles, they can create multiple paths to the receiver. These signals can interfere with each other and cause errors in the position calculation. All these factors combined lead to the GNSS positional errors varying across different locations in urban environments.

Such variance highlights the importance of context-considered and adaptive prediction of the GNSS positional errors, which can also be cross validated by the results in this study. The baseline methods (BAEE, AUB, UB) generate the uncertain regions based on the spatial and temporal distance between sample points, meaning that the sample points with similar distance can generate similar uncertain regions, regardless of locating in distinct urban environments. Fig. 11 (b)-(c), shows that the predicted point-wise GNSS positional errors by baseline methods basically stay in stable level, despite the significant fluctuations in actual GNSS positional errors across different locations, which causes the baseline methods' underperformance and less preciseness in predicting positional errors. In comparison, Fig. 11 (a) shows the predicted errors by our methods can very well approximate the actual GNSS positional errors regarding shapes and scale, demonstrating our method's advantage in adaptively and hence precisely predicting the GNSS positional errors with consideration of varying sampling and measurement errors.

### 4.2. Limitations of current uncertainty prediction model

The developed Bi-LSTM-based human movement uncertainty modeling framework aims to model crowdsourced human trajectories. However, it faces certain limitations in daily-life mobile applications,

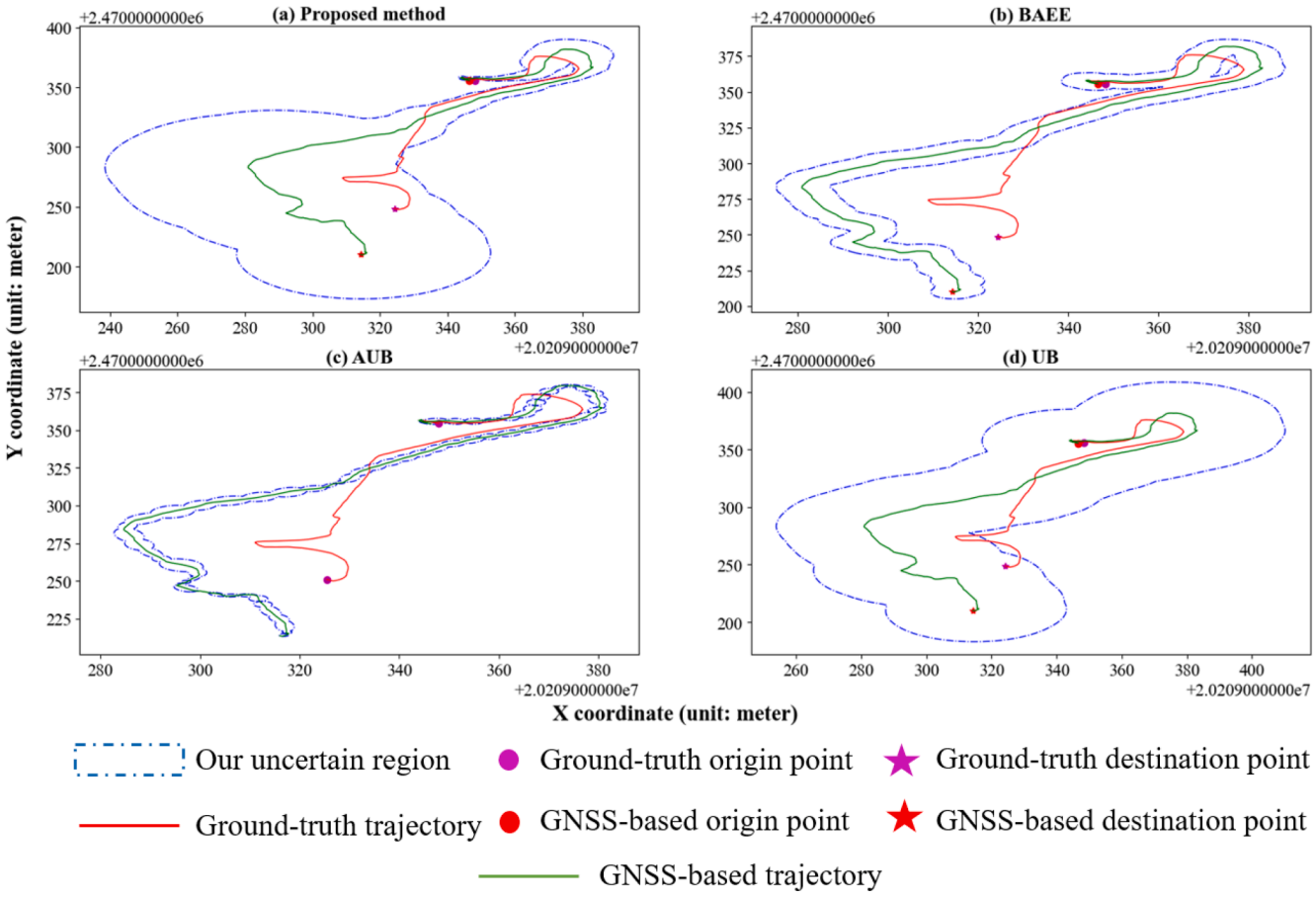


**Fig. 9.** A snapshot of the uncertain regions generated by (a) our proposed method, (b) BAEE, (c) AUB, (d) UB, on one sample trajectory.

**Table 2**
Coverage ratio of respective method on each trajectory.

| | Coverage Ratio | | | |
|---|---|---|---|---|
| | Proposed method | BAEE | AUB | UB |
| 1 | 94.7 % | 59.6 % | 70.2 % | 88.4 % |
| 2 | 97.5 % | 21.7 % | 23.8 % | 100 % |
| 3 | 100 % | 29.7 % | 35.2 % | 81.7 % |
| 4 | 83.8 % | 56.9 % | 61.0 % | 100 % |
| 5 | 96.8 % | 50.2 % | 15.2 % | 100 % |
| 6 | 100 % | 74.3 % | 36.0 % | 100 % |
| 7 | 97.9 % | 83.8 % | 64.9 % | 94.0 % |
| 8 | 100 % | 66.8 % | 51.5 % | 100 % |
| 9 | 97.5 % | 67.7 % | 52.3 % | 100 % |
| 10 | 100 % | 82.9 % | 59.5 % | 100 % |
| 11 | 98.2 % | 78.2 % | 23.6 % | 100 % |
| 12 | 100 % | 87.4 % | 46.7 % | 100 % |
| 13 | 99.0 % | 34.5 % | 48.7 % | 100 % |
| 14 | 99.5 % | 57.8 % | 32.8 % | 100 % |
| 15 | 99.3 % | 82.1 % | 46.9 % | 100 % |
| **Average** | 98.1 % | 68.2 % | 38.2 % | 97.9 % |

**Table 3**
MAE of respective method on each trajectory.

| | MAE (meter) | | | |
|---|---|---|---|---|
| Trajectory | Proposed method | BAEE | AUB | UB |
| 1 | 0.95 | 13.36 | 14.13 | 37.30 |
| 2 | 2.63 | 54.41 | 54.41 | 21.62 |
| 3 | 1.69 | 50.92 | 51.78 | 15.52 |
| 4 | 1.34 | 7.10 | 7.56 | 44.20 |
| 5 | 1.58 | 31.95 | 32.39 | 29.23 |
| 6 | 1.31 | 7.01 | 9.39 | 43.15 |
| 7 | 2.53 | 12.05 | 13.41 | 47.09 |
| 8 | 2.32 | 12.05 | 10.98 | 41.90 |
| 9 | 2.15 | 7.57 | 8.73 | 47.96 |
| 10 | 2.10 | 9.63 | 10.61 | 44.80 |
| 11 | 1.23 | 4.10 | 5.70 | 45.83 |
| 12 | 1.83 | 7.95 | 8.86 | 44.97 |
| 13 | 1.86 | 10.04 | 11.28 | 43.62 |
| 14 | 1.98 | 8.16 | 9.63 | 47.22 |
| 15 | 1.73 | 8.25 | 9.66 | 45.68 |
| **Average** | 1.82 | 16.30 | 17.23 | 40.00 |

particularly under changeable and disturbance urban areas. These limitations include the following points:

Firstly, human movement trajectories always contains both indoor and outdoor parts, while the GNSS signal is often weak or unavailable indoors. To address this challenge, it is essential to consider seamless localization trajectories that take into account both indoor and outdoor motion features. A more robust and expressive uncertainty prediction structure is required to achieve this goal.

In addition, the accuracy of the final uncertainty prediction depends on the input vector of the deep-learning model and the richness of the generated dataset. Therefore, incorporating additional trajectory-related features could enhance the performance for final uncertainty region prediction. Furthermore, obtaining accurate labels for the training dataset can be difficult, especially for ground-truth trajectories in indoor areas. In these cases, unsupervised learning could be a useful method for autonomously learning uncertainty-related trajectory features and acquiring optimal models.

Besides, there are some potential state-of-the-art models that can be used to further improve the performance of our models, especially those borrowed from Natural Language Processing (NLP), as both of our

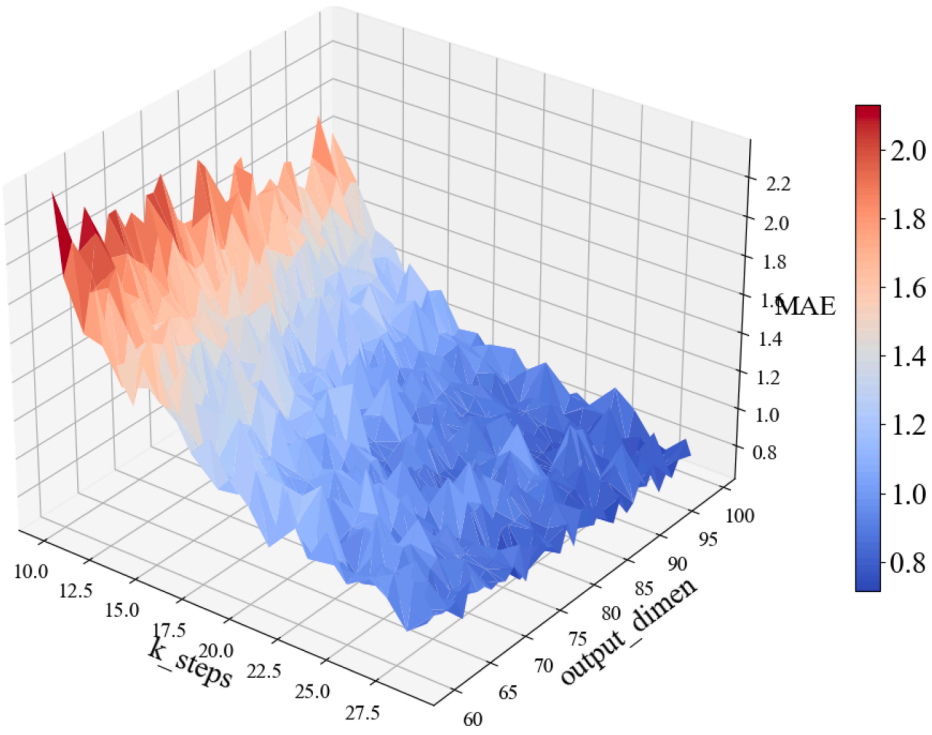


**Fig. 10.** Hyperparameter sensitivity analysis: the fluctuation of model performance under different hyperparameter selection.

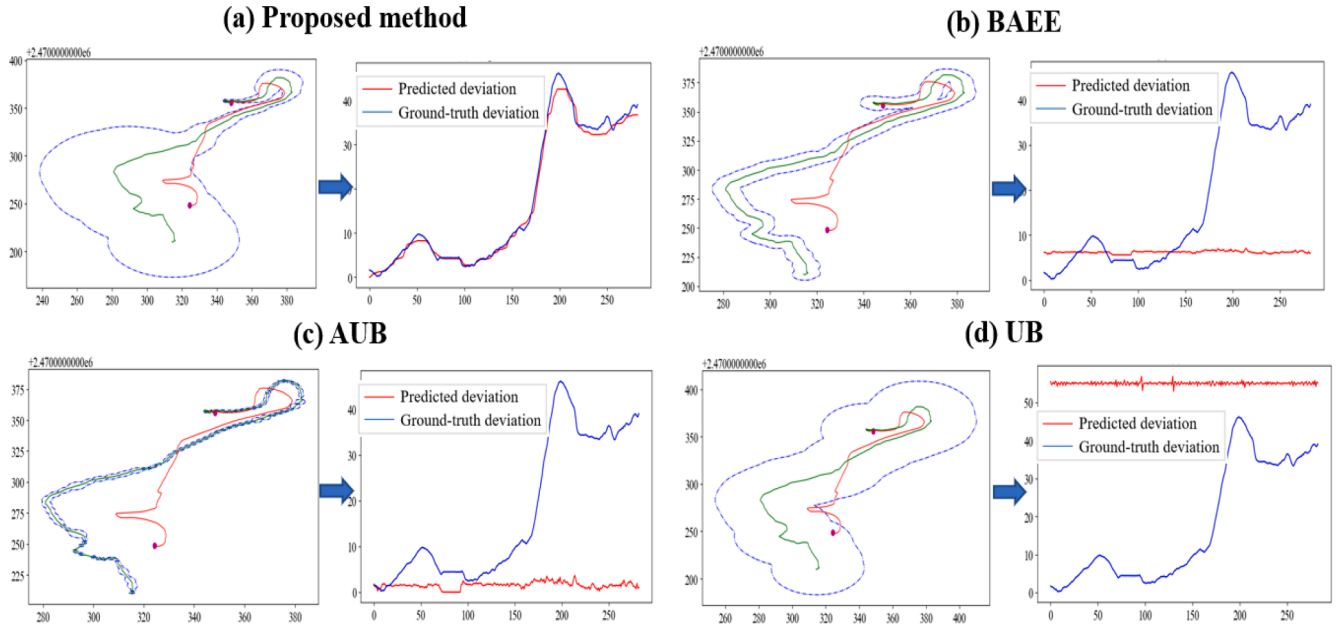


**Fig. 11.** The uncertain region and point-wise ground-truth/predicted errors on one sample trajectory.

uncertainty error prediction and the NLP problems can be formulated as sequence prediction. One potential future direction is thus to do first do feature embedding and then apply transformer-based structure, such as GPT (Generative Pre-trained Transformer) (Radford et al., 2018) or BERT (Bidirectional Encoder Representations from Transformers) (Devlin et al., 2018), for our problem solving. These models have demonstrated impressive performance in various tasks, showcasing their ability to accurately predict the next element in a sequence. This opens up new possibilities for improving the performance of our problem and other applications.

Moreover, various location sources exist in both indoor and outdoor environments, including different kinds of RF signals and local fields, which can serve as observations and input vector for compensation of indoor human motion analytics and more accurate movement uncertainty modelling. Thus, the future work of uncertainty analytics of human trajectory focuses on combining extracted and self-learned features from various mobile sensing and positioning sources comprehensively. This would improve the precision of final uncertainty area modelling by considering more supporting sources. Furthermore, it is crucial to consider and model the relationship between different mobile sensing and positioning sources. Automatically incorporating these mapping relationships into the uncertainty prediction model is essential

for obtaining optimal uncertainty estimation results.

## 5. Conclusion

Crowdsourced human trajectories play a crucial role in the development of mobile sensing and positioning applications. However, the uncertainty associated with pedestrian movement trajectories can significantly impact the accuracy of the analysis of large-scale spatio-temporal data in urban areas. Traditional uncertainty prediction structures mainly focus on constant sampling or measurement errors, which may not always be effective in real-world scenarios.

To address this challenge, we propose a Bi-LSTM-based framework that enables accurate uncertainty error and uncertainty areas modelling for crowdsourced human motion trajectories in large-scale urban environments. Our model considers both sampling and measurement errors and utilizes rich extracted features from extensive daily-life trajectories as input vectors. Moreover, our model achieves high adaptability by considering a sequence of measured vectors instead of solely adjacent measurements.

We evaluate the effectiveness of our proposed model using a real-world training dataset collected in complex urban areas that contain sampling and measurement errors. The robustness of our model's uncertainty prediction accuracy is demonstrated through various accuracy measurements, including an average Euclidean error distance of less than 1.82 m and a coverage ratio of more than 98.1 %. These results have significant implications for mobile applications in smart cities and public analytics.

## 6. Fundings

This work was supported by The Hong Kong Polytechnic University (Otto Poon Charitable Foundation Smart Cities Research Institute, Work Program: P0045937, CD03; 1-ZVN6). This research was also funded by Wuhan University, State Key Laboratory of Information Engineering in Surveying Mapping and Remote Sensing (21S02).

## 7. Data availability

Data will be made available on request.

## CRediT authorship contribution statement

**Yue Yu:** Conceptualization, Methodology, Software, Validation, Formal analysis, Writing – original draft, Writing – review & editing, Supervision, Project administration, Funding acquisition. **Yepeng Yao:** Conceptualization, Methodology, Software, Validation, Formal analysis, Writing – original draft, Writing – review & editing. **Zhewei Liu:** Conceptualization, Methodology, Software, Validation, Formal analysis, Writing – original draft, Writing – review & editing. **Zhenlin An:** Conceptualization, Methodology, Validation, Formal analysis. **Biyu Chen:** Conceptualization, Methodology, Validation, Formal analysis. **Liang Chen:** Project administration, Writing – review & editing. **Ruizhi Chen:** Supervision, Project administration, Methodology, Writing – review & editing.

## Declaration of Competing Interest

The authors declare that they have no known competing financial interests or personal relationships that could have appeared to influence the work reported in this paper.

## Data availability

Data will be made available on request.

## References

Bao, S., Shi, W., Chen, P., et al., 2022. A systematic mapping framework for backpack mobile mapping system in common monotonous environments. Measurement 197, 111243.

Devlin, J., Chang, M.W., Lee, K. and Toutanova, K., 2018. Bert: Pre-training of deep bidirectional transformers for language understanding. arXiv preprint arXiv: 1810.04805.

Downs, J.A., Horner, M.W., 2014. Adaptive-velocity time-geographic density estimation for mapping the potential and probable locations of mobile objects[J]. Environ. Plann. B. Plann. Des. 41 (6), 1006–1021.

Furtado, A.S., et al., 2018. Unveiling movement uncertainty for robust trajectory similarity analysis. Int. J. Geogr. Inf. Sci. 32 (1), 140–168.

Huang, X., Wang, S., Zhang, M., et al., 2022. Social media mining under the COVID-19 context: Progress, challenges, and opportunities. Int. J. Appl. Earth Obs. Geoinf. 113, 102967.

Kwan, M.P., 1998. Space-time and integral measures of individual accessibility: a comparative analysis using a point-based framework[J]. Geogr. Anal. 30 (3), 191–216.

Li, H., Lu, H., Shou, L., et al., 2018. In search of indoor dense regions: An approach using indoor positioning data. IEEE Trans. Knowl. Data Eng. 30 (8), 1481–1495.

Li, Z., Zhao, X., Zhao, Z., et al., 2021. WiFi-RITA positioning: Enhanced crowdsourcing positioning based on massive noisy user traces. IEEE Trans. Wirel. Commun. 20 (6), 3785–3799.

Liu, C., Feng, Y., Lin, D., et al., 2020. Iot based laundry services: an application of big data analytics, intelligent logistics management, and machine learning techniques. Int. J. Prod. Res. 58 (17), 5113–5131.

Liu, Z., Zhou, X., Shi, W., et al., 2018. Towards detecting social events by mining geographical patterns with VGI data[J]. ISPRS Int. J. Geo Inf. 7 (12), 481.

Liu, Z., Shi, W., Zhang, A., 2021. Detecting home countries of social media users with machine-learned ranking approach: a case study in Hong Kong. Appl. Geogr. 134, 102532.

Liu, Z., Zhang, A., Yao, Y., et al., 2021. Analysis of the performance and robustness of methods to detect base locations of individuals with geo-tagged social media data [J]. Int. J. Geogr. Inf. Sci. 35 (3), 609–627.

Liu, Z., Liu, J., Huang, X., Zhang, E., Chen, B., 2022. Measuring Chinese cities' economic development with mobile application usage. J. Geog. Sci. 32 (12), 2415–2429.

Liu, Z., Shi, W., Yu, Y., et al., 2022. A LSTM-based approach for modelling the movement uncertainty of indoor trajectories with mobile sensing data. Int. J. Appl. Earth Obs. Geoinf. 108, 102758.

Liu, Z., Wang, A., Weber, K., et al., 2022. Categorisation of cultural tourism attractions by tourist preference using location-based social network data: The case of Central, Hong Kong. Tourism Manage. 90, 104488.

Lu, H., Guo, C., Yang, B., et al. Finding Frequently Visited Indoor POIs Using Symbolic Indoor Tracking Data[C]//EDBT. 2016: 449-460.

Miller, H.J., 1991. Modelling accessibility using space-time prism concepts within geographical information systems[J]. Int. J. Geogr. Inform. Syst. 5 (3), 287–301.

Radford, A., Narasimhan, K., Salimans, T. and Sutskever, I., 2018. Improving language understanding by generative pre-training.

Rossi, L., Paolanti, M., Pierdicca, R., et al., 2021. Human trajectory prediction and generation using LSTM models and GANs. Pattern Recogn. 120, 108136.

Ruizhi, C., Liang, C., 2017. Indoor Positioning with Smartphones: The State-of-the-art and the Challenges. Acta Geodaetica et Cartographica Sinica 46 (10), 1316.

Shi, W., Chen, P., Shen, X., et al., 2021. An adaptive approach for modelling the movement uncertainty in trajectory data based on the concept of error ellipses[J]. Int. J. Geogr. Inf. Sci. 35 (6), 1131–1154.

Shi, W., Liu, Z., An, Z., Chen, P., 2021. RegNet: a neural network model for predicting regional desirability with VGI data. Int. J. Geogr. Inf. Sci. 35 (1), 175–192.

Shi, W., Yu, Y., Liu, Z., et al., 2022. A deep-learning approach for modelling pedestrian movement uncertainty in large-scale indoor areas. Int. J. Appl. Earth Obs. Geoinf. 114, 103065.

https://studylib.net/doc/5866728/the-average-distance-in-an-ellipse.

Tu, W., Mai, K., Zhang, Y., et al., 2020. Real-time route recommendations for E-taxies leveraging GNSS trajectories. IEEE Trans. Ind. Inf. 17 (5), 3133–3142.

Wen, W.S., Hsu, L.T., 2022. 3D LiDAR aided GNSS NLOS mitigation in urban canyons. IEEE Trans. Intell. Transp. Syst. 23 (10), 18224–18236.

Xia, F., Wang, J., Kong, X., et al., 2018. Exploring human mobility patterns in urban scenarios: A trajectory data perspective[J]. IEEE Commun. Mag. 56 (3), 142–149.

Yu, Y., Chen, R., Chen, L., et al., 2021. H-WPS: Hybrid wireless positioning system using an enhanced wi-fi FTM/RSSI/MEMS sensors integration approach. IEEE Internet Things J. 9 (14), 11827–11842.

Yu, Y., Shi, W., Chen, R., et al., 2022. Map-Assisted Seamless Localization Using Crowdsourced Trajectories Data and Bi-LSTM Based Quality Control Criteria. IEEE Sens. J. 22 (16), 16481–16491.

Yu, Y., Chen, R., Shi, W., et al., 2022. Precise 3D indoor localization and trajectory optimization based on sparse Wi-Fi FTM anchors and built-in sensors. IEEE Trans. Veh. Technol. 71 (4), 4042–4056.

Zheng, K., et al., 2012. Reducing uncertainty of low-sampling-rate trajectories. In: 2012 IEEE 28th international conference on data engineering. Arlington, Virginia, pp. 1144–1155.

Zheng, Y., 2015. Trajectory data mining: an overview. ACM Trans. Intell. Syst. Technol. (TIST) 6 (3), 29.

Zheng, Z., Rasouli, S., Timmermans, H., 2014. Evaluating the accuracy of GNSS-based taxi trajectory records. Proc. Environ. Sci. 22, 186–198.

Zhou, X., Luo, Q., Zhang, D., et al. Detecting taxi speeding from sparse and low-sampled trajectory data[C]//Asia-Pacific Web (APWeb) and Web-Age Information

Management (WAIM) Joint International Conference on Web and Big Data. Springer, Cham, 2018: 214-222.